Mechanism and Machine Theory 215 (2025) 106168

Contents lists available at ScienceDirect

Mechanism and Machine Theory

journal homepage: www.elsevier.com/locate/mechmt

Research paper

Application of rack method in generation of internally geared rotor profiles☆

Halil Lacevic *, Ahmed Kovacevic, Nikola Stosic, Matthew Read

Centre for Compressor Technology, City St George's University, Northampton Square, EC1V 0HB London, United Kingdom

ARTICLE INFO

Keywords:
Rotor profiling
Gerotor
Internally geared screw machine
Rack method
Pdm

ABSTRACT

This study explores the application of the rack method, traditionally used for generating rotor profiles in spur gears and twin screw compressors, to rotor profile generation of internally geared positive displacement machines. The necessary conditions for ensuring continuous contact in these profiles are examined. An analytical approach is proposed, where a rack profile based on trochoidal curves generates the inner rotor profile, from which the outer rotor profile is derived. Additionally, a numerical approach is introduced, demonstrating feasibility using a sine wave rack profile to generate the outer rotor, from which the inner rotor profile is derived. The methodology could be applied to rotor profiles with a non-zero minimum working chamber area, as found in gerotor pumps, and modified profiles with a zero minimum area, as required for internally geared screw machines. This work provides the first demonstration of general rack-generated rotor profiles for internally geared positive displacement machines. It establishes a foundation for refining the rack method and developing advanced numerical techniques for machine design and optimisation.

1. Introduction

Positive displacement machines (PDMs) are mechanical devices in which work is done on or by a fluid contained within a working chamber via displacement of the chamber boundary. These machines are widely used across various industries, including fluid transportation, hydraulic systems, refrigeration, and gas compression, due to their ability to maintain a consistent volumetric flow rate irrespective of pressure fluctuations [1,2]. If the working chamber is always exposed to either a low or high pressure port, the machine operates as a pump, continuously transporting fluid [3–5]. However, if the porting system is designed to regulate the timing of fluid intake and discharge, fluid is contained within a working chamber while the volume changes, and the machine can therefore function as a gas compressor or expander [6–8].

Positive displacement machines can be implemented using a wide range of mechanisms and configurations. Commonly used rotary PDM configurations incorporate either externally or internally geared intermeshing rotors that form working chambers to enclose and transport fluid. In externally geared configurations, such as external gear pumps and twin-screw compressors, the rotors are enclosed within a fixed casing, forming working chambers between the rotor lobes and casing walls. Internally geared configurations, including gerotor pumps, progressive cavity pumps, and internally geared screw compressors, achieve continuous contact lines between the inner and outer rotors, creating working chambers contained between the inner and outer rotors, and stationary end surfaces if present.

☆ This document is the results of the research project funded by Carrier Global Corporation, USA and PDM Analysis Ltd, UK.
* Corresponding author.
E-mail address: halil.lacevic@citystgeorges.ac.uk (H. Lacevic).

https://doi.org/10.1016/j.mechmachtheory.2025.106168
Received 4 April 2025; Received in revised form 20 June 2025; Accepted 1 August 2025
Available online 13 August 2025

Nomenclature

N_1	Number of lobes of the main rotor
N_2	Number of lobes of the gate rotor
r_{1w}	Radius of the pitch circle of the main rotor
r_{2w}	Radius of the pitch circle of the gate rotor
m_{21}	Gearing ratio between the rotors
E	Axis distance between the rotors
S_1	Local coordinate system of the main rotor
S_2	Local coordinate system of the gate rotor
S_f	Global coordinate system
σ	General meshing angle
σ_1	Meshing angle of the main rotor
σ_2	Meshing angle of the gate rotor
θ	Profile curve parameter
$x_{r_1}^{(1)}, y_{r_1}^{(1)}$	Main rotor Cartesian coordinates in S_1
$x_{r_2}^{(2)}, y_{r_2}^{(2)}$	Gate rotor Cartesian coordinates in S_2
$x_R^{(f)}, y_R^{(f)}$	Rack profile Cartesian coordinates in S_f
$M_t^{(1)}$	Transition point between the solutions of the meshing condition

Both externally and internally geared configurations can incorporate either straight-cut rotors, as found in external gear and gerotor pumps, or helical rotors, as used in conventional twin-screw and internally geared screw compressors. The addition of helical twist can enhance compression efficiency by decreasing port velocities and decreasing pressure differences across leakage paths [9].

For externally and internally geared PDMs, a critical factor affecting performance is the precise meshing of rotors and tight manufacturing tolerances, which are essential for minimising leakage and ensuring effective sealing [10,11], while also influencing the contact mechanics and rotor wear [12,13]. This is particularly true in compression applications where low viscosity of the gaseous working fluid can lead to high leakage flow velocities [14].

Over the past decades, researchers have focused on understanding the geometry of positive displacement machines [5,15,16] and developing prediction models using either one-dimensional [14,17,18] or multi-dimensional approaches [11,19,20]. A comprehensive understanding of geometry, combined with reliable performance prediction tools, enables the optimisation of machine configurations for specific application.

The performance of positive displacement machines is highly dependent on rotor shape and machine geometry, making rotor profiling a critical factor in achieving effective designs. In gerotor and progressive cavity pumps, as well as internally geared screw machines, rotor profiles are predominantly defined using epitrochoidal curves [21,22]. In contrast, rotor profiles in conventional twin-screw compressors are typically generated using the well-established rack method [9].

The rack method has previously been applied to internal spur gears [23] where the contact mechanics and power transmission efficiency are the primary concerns. It has not, however, been thoroughly investigated for defining internally geared rotors in positive displacement machines, where continuous rotor-to-rotor contact lines are critical to ensure effective sealing of working chambers. The rack method offers advantages by enabling rotor profiles to be constructed from curve sections on the rack, providing greater control over the type of contact points between the rotors. Since rotor profile geometry directly influences key factors such as working chamber volume, port areas, contact points, and leakage areas, all of which significantly impact machine efficiency, exploring novel approaches to rotor profiling is well justified.

The aim of this paper is to establish the theoretical and geometric foundation of a novel approach to rotor profile generation by extending the rack method for use in internally geared configurations. This is an important contribution as it provides a rigorous basis for generating the necessary input geometry for optimisation of specific machine configurations and operating conditions. Integration of this rack generation method with specialist performance analysis tools is beyond the scope of the current paper, but will be the focus of future work.

2. Review of the profiling methods for meshing rotors

Rotary positive displacement machines consist of meshing rotors that create a series of working chambers. In conventional twin-screw compressors, the two meshing rotors are referred to as the main and gate rotors. For the internally geared pump or compressor configuration, the meshing rotors are referred to as the inner and outer. In this study, the inner rotor is considered to be the main rotor for the internally geared configuration.

To ensure proper meshing of the rotors, the *Fundamental Law of Gearing* (also known as the meshing condition) must be satisfied. This law states that for a pair of rotors (gears) to maintain a constant velocity ratio, the normal at the contact point of their tooth

profiles must always pass through a fixed point on the line of centres, known as the pitch point [24]. The coordinates of the pitch point, defined in the main rotor's local coordinate system, are given in Eq. (1), where $\sigma_1 = \sigma$ represents the rotational position of the main rotor. The main rotor's coordinates in its local coordinate system are provided in Eq. (2), where θ is the general rotor profile curve parameter. The normal vectors can be determined for each point on the main rotor, as shown in Eq. (3). The general equation for the meshing condition, as described by Vecchiato, Demenego, Argyris, and Litvin [22], is presented in Eq. (4). The same condition applies to the gate rotor in its local coordinate system. Eq. (4) is necessary to explore meshing solutions for a rack profile, as discussed below.

$$P_1^{(1)}(\sigma) = (P_x^{(1)}(\sigma), P_y^{(1)}(\sigma)) \tag{1}$$

$$R_1^{(1)}(\theta) = (x_{r_1}^{(1)}(\theta), y_{r_1}^{(1)}(\theta)) \tag{2}$$

$$\overrightarrow{N_1^{(1)}}(\theta) = \left[-\frac{dy_{r_1}^{(1)}(\theta)}{d\theta}, \frac{dx_{r_1}^{(1)}(\theta)}{d\theta}, 0 \right] \tag{3}$$

$$\overrightarrow{R_1 P^{(1)}}(\theta, \sigma) \times \overrightarrow{N_1^{(1)}}(\theta) = \left(x_{r_1}^{(1)}(\theta) - P_x^{(1)}(\sigma) \right) \cdot \frac{dx_{r_1}^{(1)}(\theta)}{d\theta} + \left(y_{r_1}^{(1)}(\theta) - P_y^{(1)}(\sigma) \right) \cdot \frac{dy_{r_1}^{(1)}(\theta)}{d\theta} = 0 \tag{4}$$

The meshing condition plays a crucial role in both externally and internally geared designs. The externally geared design of rotor profiles in positive displacement machines has been extensively studied and widely applied, particularly in external spur pumps and conventional twin-screw machines. The most commonly used method for generating externally geared rotor profiles involves designing a third rotor of infinite pitch radius, known as the *rack rotor*, which meshes with both the main and gate rotors. This approach, referred to as the *rack method*, is based on the principles of the *Envelope Theory* [25], originally developed within the field of differential geometry. The rack method was first introduced by Sakun [26] as a mathematical framework for defining the meshing condition, which must be satisfied by the meshing curve generated for a given pair of rotors.

Initially, the meshing condition between the rack and each rotor profile was solved analytically, imposing constraints on the selection of the meshing curve. The curve had to be analytically differentiable, limiting the options to simple geometric shapes such as circles, lines, and points. However, the advancements introduced by Stosic [9] significantly simplified the design process by proposing a numerical approach that employs central difference methods to solve the meshing condition and derive the meshing curve.

The introduction of numerical techniques to the rack method expanded the flexibility of meshing curve design, allowing for a broader range of profile shapes. This flexibility enables profile shapes to be defined through sections on the rack, facilitating the generation of various types of contact points at specific locations.

Although the meshing condition presented in Eq. (4) may have multiple solutions for a single point on the rotor, in external gearing, such as the rotor profiles used in conventional twin-screw machines, the selection of solutions is straightforward. It can be deduced that the roots of the equation always lie in the first and fourth quadrants of the rotor's local coordinate system [9]. The rack method is widely used to generate involute profiles; however, it has also played a significant role in developing highly efficient rotor profiles for conventional twin-screw machines [27]. One of its key contributions to twin-screw machines was the introduction of asymmetric rotor profiles, which improved sealing within working chambers operating under higher pressure differences.

On the other hand, internally geared designs of positive displacement machines have primarily been developed for pumping applications. The most common configurations include liquid gerotor pumps [28] and progressive cavity pumps [4].

A key difference compared to the externally geared designs is that internally geared positive displacement machines must satisfy an additional constraint to ensure continuous contact between the rotors throughout rotation, enabling proper sealing of the working chambers. This constraint further complicates the design process of internally geared positive displacement machines. Another fundamental requirement for internally geared designs is that the absolute difference between the number of lobes on the main and gate rotors must be equal to one.

The initial concept of internally geared screw compressor design originates from gerotor pumps and was first introduced by Read, Smith and Stosic [8]. The key difference in rotor profiles is that internally geared screw compressor profiles must achieve a zero-minimum working chamber area to limit leakage flows, whereas this constraint is not imperative in straight-cut gerotor machines.

Various methods based on epitrochoidal curves for generating rotor geometry in gerotor applications have been described in previous studies [21,22,28]. While these methods are primarily employed to generate rotor profiles in gerotor pumps, alternative approaches incorporating non-circular pins and deviation functions have also been explored in several studies [29–31]. More recent studies on gerotor pumps have focused on generating rotor profiles to enhance performance and minimise wear [32,33].

In earlier studies, Read et al. [8] proposed internally geared screw compressor rotor profiles based on combinations of epicycloid and hypocycloid curves, where the selection of profiles is limited. More recent studies on internally geared screw compressors [17,34,35] have adopted the method described by Vecchiato et al. [22], commonly referred to as the pin-generation method.

The method described by Vecchiato et al. [22] provides analytical solutions for generating rotors from predefined circular pins. By numerically solving the meshing condition, the method can be generalised to allow an arbitrary curve to be used as a pin [36]. Previously described methods focused on producing symmetric profiles predominantly. Asymmetric internally geared rotor profiles

for positive displacement machines were recently proposed by Read [37] where a combination of circular pins is presented. Another approach for generating asymmetric rotor profiles was introduced by Genta, Ghigo and Milanese [38], utilising elliptical pins.

While the rack method has significantly advanced rotor design in traditional screw compressors, it has not been extensively studied for application in internally geared designs. An initial investigation into the application of the rack method to internally geared designs was introduced by Lacevic, Kovacevic, Stosic and Read [39], where a combination of cycloid and inverted cycloid curves was used as the rack profile. The condition of continuous contact was naturally satisfied due to the properties of cycloidal curves.

Since the rack method has provided numerous benefits to externally geared conventional twin-screw compressors, this paper aims to present a more general approach for applying the rack method to internally geared positive displacement designs, addressing both pumping and compression applications.

3. Existence of the continuous contact

The meshing condition presented in Eq. (4) can be challenging to solve analytically. However, it can also be effectively addressed through geometrical analysis, as initially described by Buckingham [40]. To enhance the understanding of continuous contact between the rotors, this section presents a detailed geometrical analysis of the meshing condition.

Consider a general lobe curve of the main rotor, as illustrated in Fig. 1(a). A representative point C on the main rotor has coordinates $(x_{r_1}^{(1)}(\theta), y_{r_1}^{(1)}(\theta))$ in the rotor's local coordinate system.

The normal at point C can be calculated using the first derivative of the rotor profile curve, and the normal angle, ψ_1, is determined as shown in Eq. (5). The polar coordinates of the rotor in its local coordinate system are given by Eq. (6).

$$\psi_1(\theta) = \tan^{-1}\left(\frac{-dx_{r_1}^{(1)}(\theta)}{dy_{r_1}^{(1)}(\theta)}\right) \tag{5}$$

$$\begin{aligned}\varphi_{p_1}(\theta) &= \tan^{-1}\left(\frac{y_{r_1}^{(1)}(\theta)}{x_{r_1}^{(1)}(\theta)}\right)\\ \rho_{p_1}(\theta) &= \sqrt{(x_{r_1}^{(1)}(\theta))^2 + (y_{r_1}^{(1)}(\theta))^2}\end{aligned} \tag{6}$$

The first solution of the meshing condition, denoted by the angle $\sigma = \sigma_1$, must be determined. Triangle $\triangle ABC$, illustrated in Fig. 1(a), can be isolated and analysed, as shown in Fig. 1(b). Using geometric principles, the corresponding angles within $\triangle ABC$ are defined and expressed in Eqs. (7).

$$\begin{aligned}\varphi_c(\theta) &= \psi_1(\theta) - \varphi_{p_1}(\theta)\\ \gamma(\theta) &= \pi - (\psi_1(\theta) - \sigma)\end{aligned} \tag{7}$$

By applying the sine rule in triangle $\triangle ABC$ (as shown in Eq. (8)) and incorporating the relationships defined in Eq. (7), the angle of the contact point, σ, can be calculated. The first solution for the meshing angle of a rotor point is provided in Eq. (9).

This solution of the meshing condition corresponds to the one used in the rack method, which lies in the first or fourth quadrant of the coordinate system. The second potential solution, which lies in the second or third quadrant, is shown in Eq. (10).

$$\begin{aligned}\frac{\sin(\varphi_c(\theta))}{r_{1_w}} &= \frac{\sin(\gamma(\theta))}{\rho_{p_1}(\theta)}\\ \gamma(\theta) &= \sin^{-1}\left(\frac{\rho_{p_1}(\theta)}{r_{1_w}} \cdot \sin(\varphi_c(\theta))\right)\end{aligned} \tag{8}$$

$$\sigma(\theta) = \psi_1(\theta) - \gamma(\theta) \tag{9}$$

$$\sigma^*(\theta) = \psi_1(\theta) + \gamma(\theta) - \pi \tag{10}$$

The meshing angles σ and σ^* alone do not constitute a sufficient condition to ensure continuous contact between the rotors. They provide an analytical means of defining the potential meshing angles at rotor points. However, to maintain continuous contact, the transition between the roots of the meshing equation must be smooth. This requires a transition point M_t at which both solutions coincide.

In other words, at the transition point, $\sigma = \sigma^*$, or equivalently, solving Eqs. (9) and (10) indicates that $\gamma = \frac{\pi}{2}$. To ensure continuous contact, the solutions for the angle γ, as described in Eq. (8), must remain continuous across the entire domain.

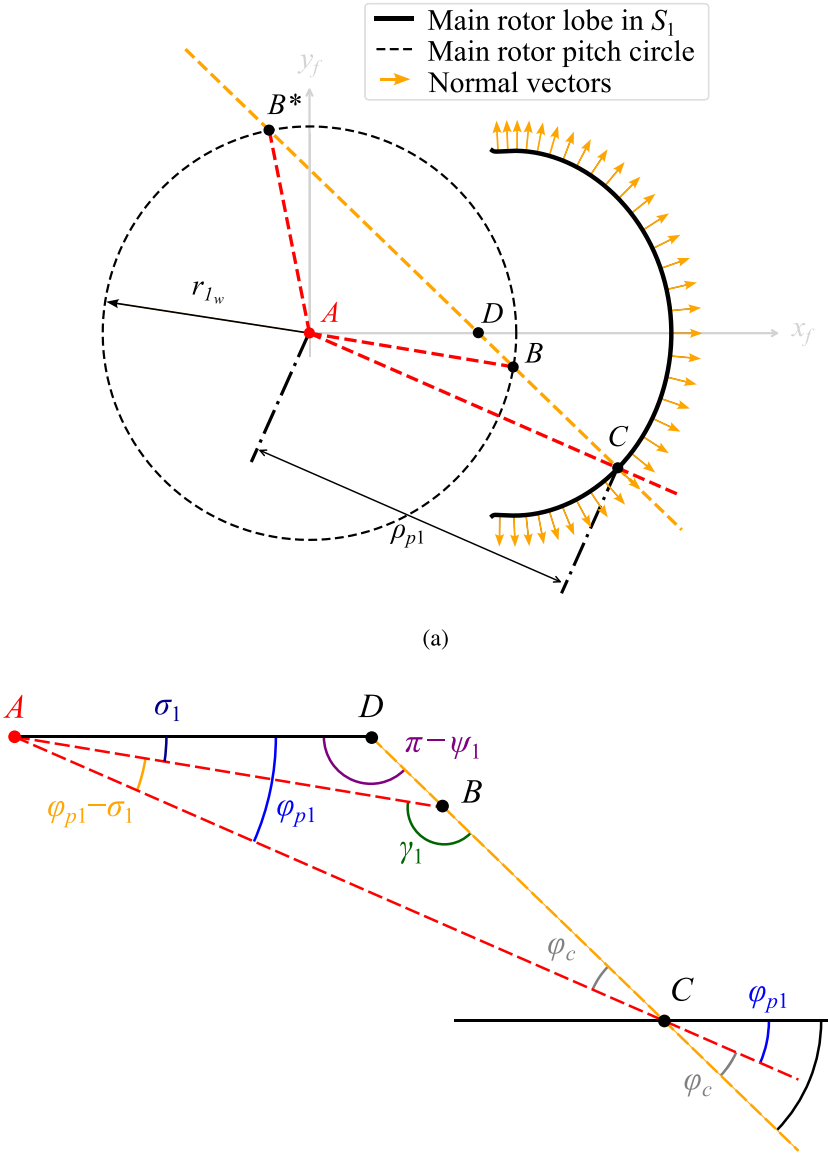

Fig. 1. Geometrical interpretation of the meshing condition: (a) a single lobe on the main rotor profile, and (b) a close-up view of triangle $\triangle ABC$.

4. Generating internally geared profiles using rack method

Since the initial rack method described by Stosic [9] does not account for the second root of the meshing equation, as described geometrically in Section 3, continuous contact cannot be guaranteed. An initial investigation conducted by Lacevic et al. [39] incorporated a combination of cycloid and inverted cycloid curves on the rack, resulting in fully valid internally geared rotor profiles that ensure both continuous contact and a zero-minimum working chamber area. However, the rack described in this initial investigation most likely represents a special case due to the inherent properties of cycloidal curves. This section presents an extended approach using the rack method to generate one rotor, which can then be used to derive the corresponding rotor. A special case, where the rack is based on a trochoidal curve and the meshing condition is solved analytically, is described alongside the general approach for generating valid internally geared rotors, with or without a zero-minimum working chamber area.

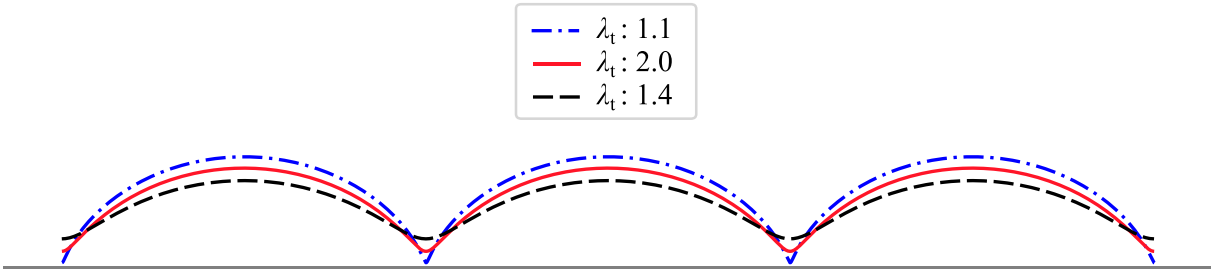

Fig. 2. Rack profiles generated from trochoid curve.

4.1. Analytical solution for trochoidal racks

The coordinates of the rack, derived from the trochoid curve, in its local coordinate system are defined in Eq. (11), where $b_t = a_t/\lambda_t$, k_t is an adjustable shape parameter, and a_t is the radius of the rolling circle, which must satisfy the gearing ratio between the rack and the main rotor as $a_t = r_{1w}N_1$. Here, r_{1w} is the pitch circle radius, and N_1 is the number of lobes of the main rotor.

The non-dimensional parameter λ_t characterises the type of trochoid curve, with this study focusing on curtate trochoid curves that satisfy the condition $\lambda_t > 1$ to ensure physically valid rack profiles. Examples of rack profiles generated by trochoid curves for different values of λ_t with $k_t = 0$ are illustrated in Fig. 2. The local coordinates of the rack profile are transformed into the global coordinate system S_f by applying the transformation matrix M_{rf} (Eq. (12)) as shown in Eq. (13). A single lobe of the rack profile is generated for $\theta \in [0, 2\pi]$, where θ serves as the general profile curve parameter. The rack curve is fully differentiable over its entire domain.

$$\begin{aligned} x_R^{(L)}(\theta) &= a_t\theta - (a_t/\lambda_t)\sin\theta \\ y_R^{(L)}(\theta) &= a_t - (a_t/\lambda_t)\cos\theta + k_t \end{aligned} \tag{11}$$

$$M_{rf} = \begin{bmatrix} 1 & 1 & 0 & r_{1_w} \\ -1 & 1 & 0 & 0 \\ 0 & 0 & 1 & 0 \\ 0 & 0 & 0 & 1 \end{bmatrix} \tag{12}$$

$$\begin{bmatrix} x_R^{(f)}(\theta) & y_R^{(f)}(\theta) & 0 & 1 \end{bmatrix} = M_{rf} \begin{bmatrix} x_R^{(L)}(\theta) & y_R^{(L)}(\theta) & 0 & 1 \end{bmatrix}^\top \tag{13}$$

The coordinates of the rack generated main (inner) rotor can be derived from the rack profile by combining the global rack coordinates, obtained from Eq. (13), with the solutions to the meshing condition between the rack profile and the main rotor profile, as described by Stosic [9] and given in Eq. (14). This relationship can be expressed and solved in matrix form, as shown in Eq. (15), where the matrix $M_{R_1}(\sigma_{r_1})$ defines the transformation from the rack coordinate system to the main rotor's local coordinate system, as presented in Eq. (16).

$$\sigma_{r_1}(\theta) = \frac{y_R^{(f)}(\theta) - \frac{dy_R^{(f)}(\theta)}{dx_R^{(f)}(\theta)}(r_{1_w} - x_R^{(f)}(\theta))}{r_{1_w}} \tag{14}$$

$$\begin{bmatrix} x_{r_1}^{(1)}(\theta, \sigma_{r_1}) & y_{r_1}^{(1)}(\theta, \sigma_{r_1}) & 0 & 1 \end{bmatrix} = M_{R_1}(\sigma_{r_1}) M_{rf} \begin{bmatrix} x_R^{(L)}(\theta) & y_R^{(L)}(\theta) & 0 & 1 \end{bmatrix}^\top \tag{15}$$

$$M_{R_1}(\sigma_{r_1}) = \begin{bmatrix} \cos\sigma_{r_1} & -\sin\sigma_{r_1} & 0 & r_{1_w}\sigma_{r_1}\sin\sigma_{r_1} \\ \sin\sigma_{r_1} & \cos\sigma_{r_1} & 0 & -r_{1_w}\sigma_{r_1}\cos\sigma_{r_1} \\ 0 & 0 & 1 & 0 \\ 0 & 0 & 0 & 1 \end{bmatrix} \tag{16}$$

Since the gate (outer) rotor in this approach does not necessarily need to mesh with the rack profile, it is essential to determine the gearing ratio in terms of the axis distance E between the rack generated main rotor and the corresponding gate rotor that satisfies the continuous contact condition. The meshing condition for the generated main rotor profile can be established using Eq. (17).

The transition point $M_t^{(1)} = (x_{r_1}^{(1)}(\theta_t), y_{r_1}^{(1)}(\theta_t))$, introduced in Section 3, can be identified in the main rotor's local coordinate system S_1 as the maximum of the function $\gamma(\theta)$, as defined in Eq. (18).

$$\gamma(\theta) = \sin^{-1}\left(\frac{\rho_{p_1}(\theta)}{N_1 E}\sin(\varphi_c(\theta))\right) \tag{17}$$

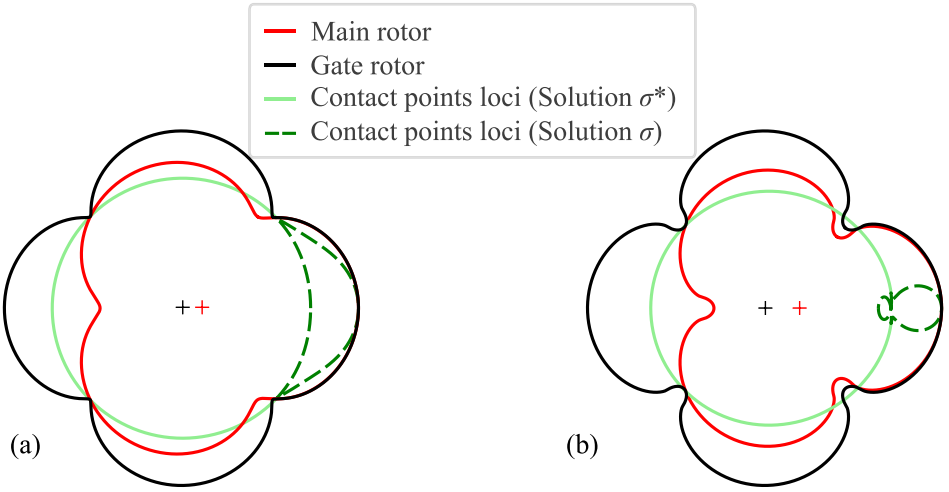

Fig. 3. Examples of internally geared rotor profiles with (a) $\lambda_t = 1.2$, $k_t = -0.5$ and (b) $\lambda_t = 1.2$, $k_t = 1$, where the main rotor profile is generated using a trochoid-based rack, and the gate rotor is derived from the corresponding main rotor profile ($N_1 = 3$, $N_2 = 4$).

$$\begin{aligned} &\frac{d\gamma(\theta)}{d\theta}(\theta_t) = 0 \\ &\rho_{p_1}(\theta_t)\frac{d\varphi_c(\theta)}{d\theta}(\theta_t)\cos(\varphi_c(\theta_t)) + \sin(\varphi_c(\theta_t))\frac{d\rho_{p_1}(\theta)}{d\theta}(\theta_t) = 0 \end{aligned} \tag{18}$$

The corresponding axis distance E required to achieve continuous contact between the rotors can be determined with respect to the identified transition point $M_t^{(1)}$ using Eq. (19). The axis distance between the main rotor, generated by a trochoid rack, and the corresponding gate rotor that ensures continuous contact is directly related to the trochoid parameter b_t, given as $E = b_t = a_t/\lambda_t$.

$$E = \left| \frac{\rho_{p_1}(\theta_t)\sin(\varphi_c(\theta_t))}{N_1} \right| \tag{19}$$

The axis distance (E) between the main rotor, generated by the trochoid-based rack profile, and the meshing gate rotor can be used to calculate the pitch circle radii of the rotors as $r_{1w} = N_1 E$ and $r_{2w} = N_2 E$, where $N_2 = N_1 \pm 1$. Additionally, both solutions to the meshing condition can be determined using Eqs. (9), (10), and (17).

By applying the transformation between the main and gate rotor's local coordinate systems, as given in Eq. (20), along with the solutions to the meshing condition, the gate rotor profile can be derived as defined in Eq. (21). The meshing condition can be established for each point on the main rotor profile based on the profile parameter θ.

For $\theta_t \le \theta \le 2\pi - \theta_t$ (defined here as the addendum section), the main rotor profile coordinates $(x_{r_1}^{(1)}(\theta), y_{r_1}^{(1)}(\theta))$ will have two solutions to the meshing condition (Eqs. (9) and (10)), representing contact points in all four quadrants. For other points on the main rotor profile (defined here as the dedendum section), only the first solution, defined by Eq. (9), will exist.

The locations of the contact points in the global coordinate system S_f can be determined by transforming them from the main rotor's local coordinate system using the transformation matrix given in Eq. (22). Examples of valid internally geared rotors with continuous contact, where main rotor profile is generated using the rack method and gate rotor profile is derived from the main rotor profile are shown in Fig. 3.

$$M_{12}^{(I)}(\sigma) = \begin{bmatrix} \cos(\sigma(1+m_{21})) & \sin(\sigma(1+m_{21})) & 0 & E \\ -\sin(\sigma(1+m_{21})) & \cos(\sigma(1+m_{21})) & 0 & 0 \\ 0 & 0 & 1 & 0 \\ 0 & 0 & 0 & 1 \end{bmatrix} \tag{20}$$

$$\begin{bmatrix} x_{r_2}^{(2)}(\theta,\sigma) & y_{r_2}^{(2)}(\theta,\sigma) & 0 & 1 \end{bmatrix} = M_{12}(\sigma)\begin{bmatrix} x_{r_1}^{(1)}(\theta) & y_{r_1}^{(1)}(\theta) & 0 & 1 \end{bmatrix}^{\top} \tag{21}$$

$$M_{1f}^{(I)}(\sigma) = \begin{bmatrix} \cos\sigma & \sin\sigma & 0 & 0 \\ -\sin\sigma & \cos\sigma & 0 & 0 \\ 0 & 0 & 1 & 0 \\ 0 & 0 & 0 & 1 \end{bmatrix} \tag{22}$$

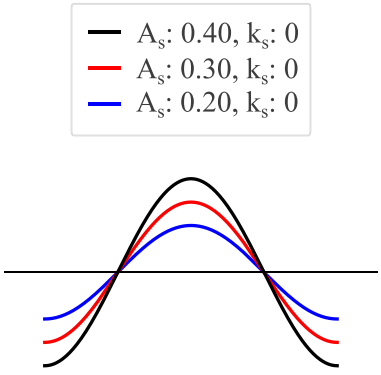

Fig. 4. Examples of rack profiles generated using sinusoidal curves with varying amplitudes and zero vertical offset ($k_s = 0$).

4.2. Numerical solution for general rack curves

A general rack curve can be defined in its local coordinate system as $x_R^{(L)}(\theta), y_R^{(L)}(\theta)$, where θ is the general profile curve parameter. Using the rack method to generate one rotor and subsequently deriving the second rotor while ensuring that the geometrical meshing condition is satisfied provides a suitable approach for generating valid rotor profiles with continuous contact.

Depending on which rotor is generated from the rack, the width of a single lobe on the rack must satisfy the gearing ratio: $r_{width} = \frac{2\pi}{N_1} r_{1w}$ if the main rotor meshes with the rack, or $r_{width} = \frac{2\pi}{N_2} r_{2w}$ if the gate rotor meshes with the rack.

In Section 4.1, the generation of the main (inner) rotor using the rack profile was described, and an analytical solution for the trochoidal rack was provided. The gate rotor was then derived from the main rotor. To emphasise the feasibility of this approach, this section describes the procedure for generating the gate (outer) rotor using the general rack profile and deriving the meshing main rotor with continuous contact.

Rack coordinates can be expressed in the global coordinate system using Eq. (13), while the coordinates of the gate rotor in its local coordinate system S_2 can be determined by applying transformational matrix defined in Eq. (23) as shown in Eq. (24), where $\sigma_{r_2} = m_{21}\sigma_{r_1}$.

$$M_{R_2}(\sigma_{r_2}) = \begin{bmatrix} \cos(m_{21}\sigma_{r_2}) & -\sin(m_{21}\sigma_{r_2}) & 0 & r_{2_w} m_{21}\sigma_{r_2} \sin(m_{21}\sigma_{r_2}) \\ \sin(m_{21}\sigma_{r_2}) & \cos(m_{21}\sigma_{r_2}) & 0 & -r_{2_w} m_{21}\sigma_{r_2} \cos(m_{21}\sigma_{r_2}) \\ 0 & 0 & 1 & 0 \\ 0 & 0 & 0 & 1 \end{bmatrix} \tag{23}$$

$$\begin{bmatrix} x_{r_2}^{(2)}(\theta,\sigma_{r_2}) & y_{r_2}^{(2)}(\theta,\sigma_{r_2}) & 0 & 1 \end{bmatrix} = M_{R_2}(\sigma_{r_2}) M_{rf} \begin{bmatrix} x_R^{(L)}(\theta) & y_R^{(L)}(\theta) & 0 & 1 \end{bmatrix}^{\top} \tag{24}$$

The existence of continuous contact between the generated gate rotor and the desired main rotor for a given gearing ratio can be ensured by numerically solving Eq. (25) for the axis distance E, where θ_t, representing the location of the transition point, is determined from Eq. (18).

$$\gamma_2(\theta_t) = \sin^{-1}\left(\frac{\rho_{p_2}(\theta_t)}{N_2 E}\sin(\varphi_c(\theta_t))\right) \tag{25}$$

The main (inner) rotor coordinates in its local coordinate system S_1 can then be derived using Eq. (26).

$$\begin{bmatrix} x_{r_1}^{(1)}(\theta,\sigma) & y_{r_1}^{(1)}(\theta,\sigma) & 0 & 1 \end{bmatrix} = M_{12}^{-1}(\sigma) \begin{bmatrix} x_{r_2}^{(2)}(\theta) & y_{r_2}^{(2)}(\theta) & 0 & 1 \end{bmatrix}^{\top} \tag{26}$$

To demonstrate the feasibility of the proposed methodology, two distinct rack profiles are used to generate pairs of internally geared rotors. The first rack profile is constructed using a sinusoidal curve, where the amplitude of the sine wave, denoted as A_s, is a controllable parameter. Another parameter influencing the resulting rotor shape is the vertical offset, k_s, which can be applied to the y-coordinate of the rack profile in its local coordinate system. Examples of sinusoidal rack profiles generated for different amplitudes with zero offset ($k_s = 0$) in its local coordinate system are shown in Fig. 4.

The second rack profile is based on a geometric combination of two circular arcs: one arc defines the dedendum portion of the profile, while the other defines the addendum. This approach enables greater control over the curvature and overall shape of the generated profiles.

The geometry of the arc-based rack profile is defined by two non-dimensional shape parameters. The first, α_p, represents a normalised arc angle such that the true arc angle is $\alpha = \pi \cdot \alpha_p$, with $\alpha_p \in [0, 1]$. The second parameter, a_p, defines the normalised chord length of the central arc, with $a_p \in [0, 1]$. Together, these parameters control the angular span and horizontal extent of the arc segments, respectively, thereby influencing the overall profile geometry. Representation of these non-dimensional shape parameters and their influence on rack rotor shape are shown in Fig. 5(a). Examples of rack profiles generated using combinations of circular arcs for various values of the non-dimensional shape parameters a_p and α_p are presented in Fig. 5(b).

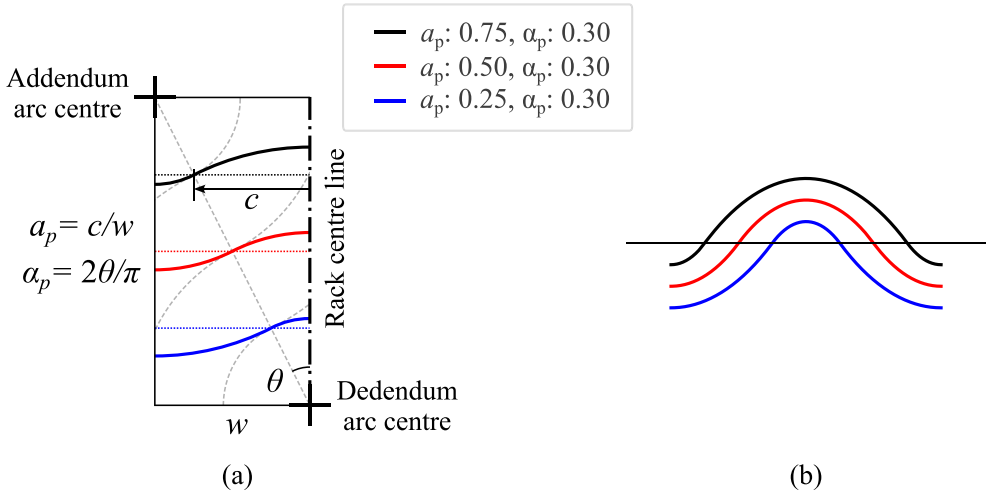

Fig. 5. Rack rotor profiles based on geometric combination of two circular arcs: (a) representation of non-dimensional shape parameters a_p and α_p; (b) rack profiles constructed using a combination of circular arcs with varying non-dimensional shape parameters α_p and a_p.

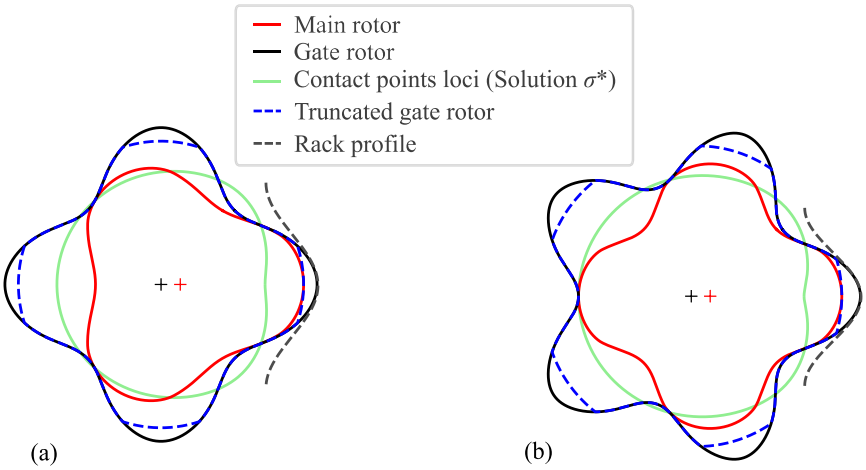

Fig. 6. Examples of internally geared rotor profiles, where (a) $N_1 = 3$, $N_2 = 4$ and (b) $N_1 = 4$, $N_2 = 5$, both achieving continuous contact and a non-zero minimum working chamber area. The profiles are generated using a sinusoidal curve (Fig. 4 where $A_s = 0.2, k_s = 0$) on the rack profile.

Examples of internally geared rotor profiles generated using sinusoidal rack profile and rack profile produced by a combination of circular arcs are shown in Fig. 6 and Fig. 7, respectively. The resulting rotors maintain continuous contact and are suitable for various applications in positive displacement machines. However, they do not necessarily provide a zero-minimum working chamber area, which is crucial for efficient compression in internally geared screw compressors.

A simple method of reducing the minimum working chamber area is to truncate the gate rotor profile using circular arc sections sized to achieve contact (or a specified gap) when the tip of the main rotor aligns with the root of the gate rotor, as shown in Figs. 6 and 7. However, if a zero-minimum working chamber area is crucial, this issue was previously addressed and resolved by Vecchiato et al. [22], and the same approach is applied in this paper. Once the meshing rotors are generated, a portion of the main (inner) rotor can be used to form the fillet part of the gate (outer) rotor, sealing the gap and ensuring a zero-minimum working chamber area, as described by Vecchiato et al. [22].

For the rack generated main rotor in Eq. (26), a corresponding fillet part of the gate rotor that ensures both continuous contact and a zero-minimum working chamber area can be defined by solving the meshing condition for the main rotor using Eq. (9) and applying Eq. (21) to determine the fillet coordinates.

Examples of fully valid internally geared rotor profiles produced from the sinusoidal curve on the rack profile (based on the profiles from Fig. 6) with both continuous contact and a zero-minimum working chamber area are shown in Fig. 8. Although this procedure is demonstrated here using profiles defined by the sinusoidal rack curve, it is equally applicable to any other rack curve formulation.

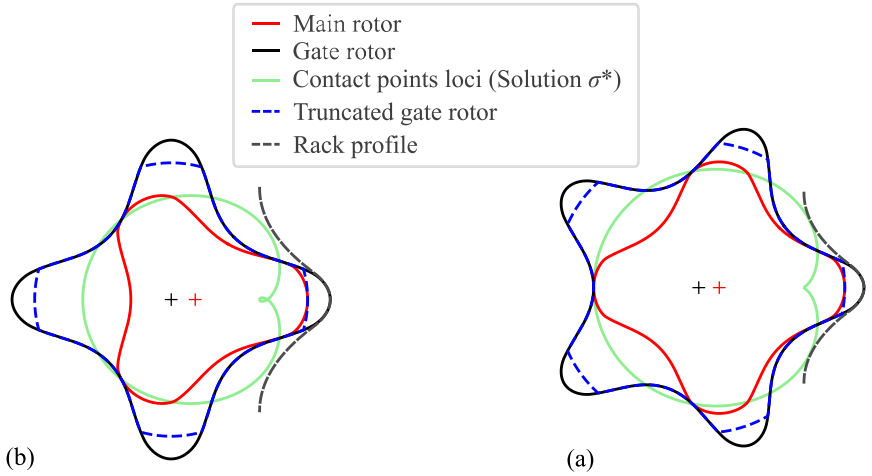

Fig. 7. Examples of internally geared rotor profiles, where (a) $N_1 = 3$, $N_2 = 4$ and (b) $N_1 = 4$, $N_2 = 5$, both achieving continuous contact and a non-zero minimum working chamber area. The profiles are generated using a combination of circular arcs (Fig. 5 where $a_p = 0.25, \alpha_p = 0.3$) on the rack profile.

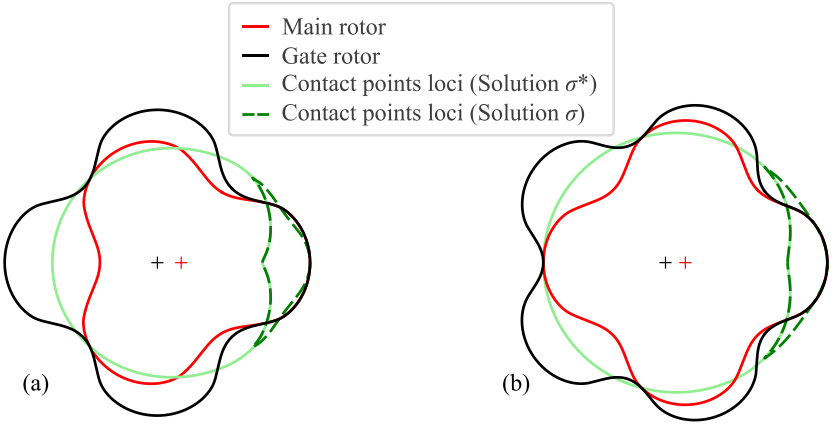

Fig. 8. Examples of the internally geared rotor profiles from Fig. 6, where (a) $N_1 = 3$, $N_2 = 4$ and (b) $N_1 = 4$, $N_2 = 5$, incorporating a modified fillet on the gate (outer) rotor to achieve a zero minimum working chamber area.

Various curve types can be applied to different sections of the rack profile, provided they result in smooth and geometrically valid rack rotor profiles. Determining the optimal combination of such curves would require detailed optimisation studies customised to specific curve families and specific engineering applications, which is beyond the scope of this paper.

4.3. Preliminary profile shape evaluation

To demonstrate the capability of the proposed methodology in enabling comparative evaluation and geometrical analysis of generated profiles, a preliminary evaluation metric is defined in terms of the relative swept volume for a gerotor pump application. For each generated rotor profile, relative swept volume, $\bar{V}_s$, is defined as the ratio of the total volume swept by the working chambers during one full rotation to the reference volume enclosed by the outer rotor tip cylinder. It provides a straightforward non-dimensional basis for comparing different profiles and supports preliminary parameter space exploration within selected families of rack generated profiles.

For rack profiles generated using sinusoidal curves (Fig. 4(a)), two shape parameters, amplitude A_s and vertical offset k_s, are varied. In the case of rack profiles constructed from a combination of circular arcs (Fig. 4(b)), the non-dimensional parameters a_p and α_p are varied within their allowable limits. The influence of these parameters on the relative swept volume is illustrated in Fig. 9(a) and (b) for the sinusoidal and circular-arc-based rack profiles, respectively. In Fig. 9, both cases show distinct regions where the relative swept volume varies as a function of the shape parameter combinations, demonstrating the influence of these parameters on the relative swept volume. In both cases, the maximum relative swept volume, $\bar{V}_s^{max}$, reaches approximately 45% of the outer rotor tip cylinder volume. The rotor profiles corresponding to the parameter combinations that produce the maximum relative swept volume for both sinusoidal and circular-arc-based rack configurations are shown in Fig. 10(a) and (b), respectively.

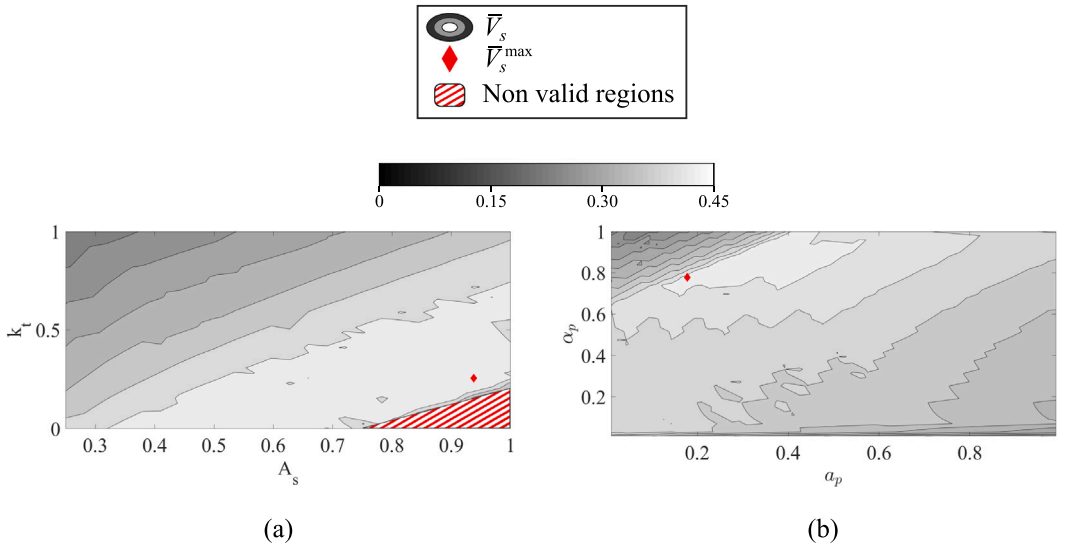

Fig. 9. Contour plots of the relative swept volume $\bar{V}_s$ as a function of rack profile parameters: (a) sinusoidal-based racks with varying amplitude A_s and vertical offset k_s; (b) circular-arc-based racks with varying non-dimensional parameters a_p and α_p.

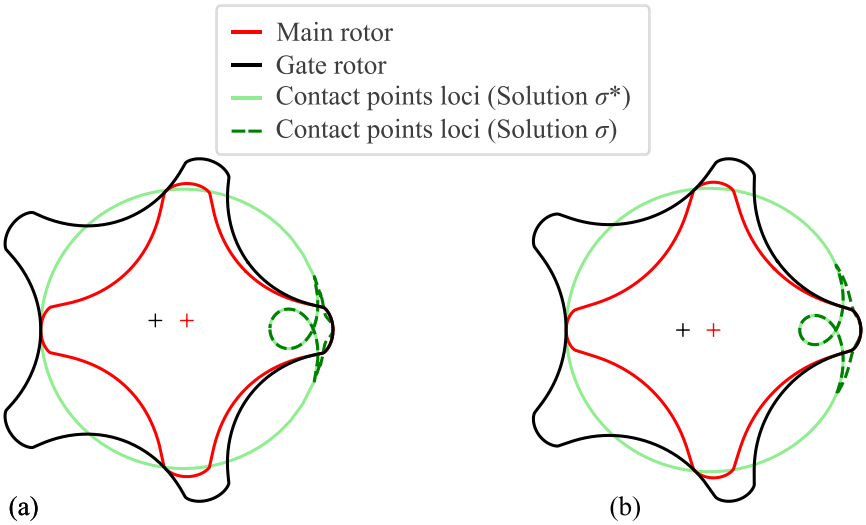

Fig. 10. Rotor profiles corresponding to the maximum relative swept volume (Fig. 9) for each rack configuration: (a) sinusoidal-based rack with $A_s = 0.94$ and $k_s = 0.26$ achieving $\bar{V}_s^{max} = 44.7\%$; (b) circular-arc-based rack with $a_p = 0.18$ and $\alpha_p = 0.78$ achieving $\bar{V}_s^{max} = 43.4\%$.

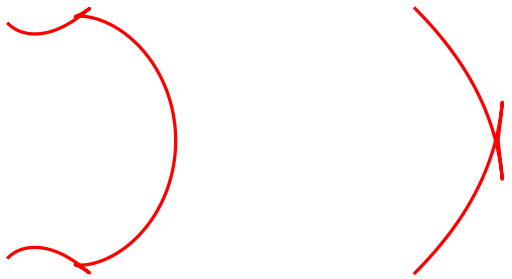

Fig. 11. Examples of undercuts that occur on the inner rotor profiles of a sinusoidal rack generated profile for non-valid regions in Fig. 9(a).

The circular-arc profiles remain valid across the entire parameter space, as evidenced by the continuous validity in Fig. 9(b). Although the sinusoidal profiles display a generally linear and smooth trend across the explored domain, some parameter combinations, however, produce undercuts that invalidate the rotor geometry (as it can be seen in Fig. 9(a) non valid region). Examples of these undercuts on the generated inner rotor profile (occurring for sinusoidal rack parameters within the invalid region) are shown in Fig. 11. These undercuts highlight limitations on parameter selection imposed by the geometrical constraints and the nature of the rack curve formulations. Such limitations must be explored in detail for specific curve families, with trends and allowable parameter bounds defined in future studies. Within this paper, the rack-curve selections serve demonstration purposes only and were not chosen based on any detailed optimisation or application-specific analysis.

5. Conclusion

This paper provides a detailed review of existing rotor profiling methods commonly used in the design of rotary positive displacement machines and examines different approaches for externally and internally geared rotor configurations. Although the rack method, widely used in conventional twin-screw machines, has been extensively applied in externally geared rotary positive displacement machines and spur gears, it has not been thoroughly investigated for internally geared rotor configurations, where maintaining continuous contact is imperative.

A geometrical solution to the meshing condition, as described in this paper, provides a sufficient condition for ensuring continuous contact between the rotors. Based on this condition, an extended approach is introduced, where the conventional rack method can be applied to generate one of the rotors. The corresponding rotor is then derived from that rotor while ensuring the continuous contact is maintained.

A special case, where the rack curve is defined as a curtate trochoid, is described in detail, and analytical solutions are presented.

Additionally, a more general approach implementing numerical solutions to the continuous contact condition is presented. This methodology is demonstrated on profiles derived from two distinct rack rotor formulations where one is based on a sinusoidal curve and the other is constructed from a combination of circular arcs. The resulting rotor profiles do not necessarily have a zero-minimum working chamber area, which is crucial for compression applications. However, an additional extension is described that modifies the gate (outer) rotor fillet, ensuring a zero-minimum working chamber area while maintaining continuous contact. Capability of the proposed methodology for geometrical analysis and comparative evaluation is illustrated by introducing a preliminary metric based on the relative swept volume and applying it to both the sinusoidal and circular-arc rack cases.

Future work will focus on understanding the limitations of the general approach and addressing potential issues related to undercuts that may occur on the rotors. The proposed approach for rotor profile generation will then be integrated with performance prediction models of real-world applications to allow optimisation of machine geometry and operating conditions.

CRediT authorship contribution statement

Halil Lacevic: Methodology, Conceptualization. **Ahmed Kovacevic:** Supervision. **Nikola Stosic:** Methodology. **Matthew Read:** Supervision.

Declaration of competing interest

The authors declare that they have no known competing financial interests or personal relationships that could have appeared to influence the work reported in this paper.

Data availability

Data will be made available on request.

References

[1] P.J. Gamez-Montero, E. Codina, R. Castilla, A review of gerotor technology in hydraulic machines, Energies 12 (12) (2019) 2423, http://dx.doi.org/10.3390/en12122423.

[2] K. Lu, I.A. Sultan, T.H. Phung, A literature review of the positive displacement compressor: Current challenges and future opportunities, Energies 16 (20) (2023) 7035, http://dx.doi.org/10.3390/en16207035.

[3] K.J. Huang, W.C. Lian, Kinematic flowrate characteristics of external spur gear pumps using an exact closed solution, Mech. Mach. Theory 44 (6) (2009) 1121–1131, http://dx.doi.org/10.1016/j.mechmachtheory.2008.10.002.

[4] N. Baroiu, G.-A. Moroşanu, V.-G. Teodor, N. Oancea, Roller profiling for generating the screw of a pump with progressive cavities, Inventions 6 (2) (2021) 34, http://dx.doi.org/10.3390/inventions6020034.

[5] C.-F. Hsieh, Y.-W. Hwang, Geometric design for a gerotor pump with high area efficiency, J. Mech. Des. 129 (12) (2006) 1269–1277, http://dx.doi.org/10.1115/1.2779887.

[6] N. Stosic, I. Smith, A. Kovacevic, Screw Compressors: Mathematical Modelling and Performance Calculation, Springer, Berlin, 2005, http://dx.doi.org/10.1007/b137216.

[7] H.A. Ohman, Test results of a screw type expander/compressor and the implication of phase separators on the refrigeration process, in: International Refrigeration and Air Conditioning Conference, (Paper 720) 2004.

[8] M.G. Read, I.K. Smith, N. Stosic, Internally geared screw machines with ported end plates, IOP Conf. Ser.: Mater. Sci. Eng. 232 (2017) 012058, http://dx.doi.org/10.1088/1757-899x/232/1/012058.
[9] N. Stosic, On gearing of helical screw compressor rotors, Proc. Inst. Mech. Eng. Part C: J. Mech. Eng. Sci. 212 (7) (1998) 587–594, http://dx.doi.org/10.1243/0954406981521556.
[10] R. Rituraj, A. Vacca, Investigation of flow through curved constrictions for leakage flow modelling in hydraulic gear pumps, Mech. Syst. Signal Process. 153 (2021) 107503.
[11] P.-J. Gamez-Montero, R. Castilla, D. del Campo, N. Ertürk, G. Raush, E. Codina, Influence of the interteeth clearances on the flow ripple in a gerotor pump for engine lubrication, Proc. Inst. Mech. Eng. Part D: J. Automob. Eng. 226 (7) (2012) 930–942.
[12] A. Robison, A. Vacca, Multi-objective optimization of circular-toothed gerotors for kinematics and wear by genetic algorithm, Mech. Mach. Theory 128 (2018) 150–168.
[13] M. Read, A methodology for investigating the influence of hydrodynamic effects in gerotor type positive displacement machines, Mech. Mach. Theory 204 (2024) 105836.
[14] K. Hanjalic, N. Stosic, Development and optimization of screw machines with a simulation model—Part II: Thermodynamic performance simulation and design optimization, J. Fluids Eng. 119 (3) (1997) 664–670, http://dx.doi.org/10.1115/1.2819296.
[15] N. Stosic, I.K. Smith, A. Kovacevic, E. Mujic, Geometry of screw compressor rotors and their tools, J. Zhejiang Univ.- Science A 12 (4) (2011) 310–326, http://dx.doi.org/10.1631/jzus.a1000393.
[16] M.G. Read, I. Smith, N. Stosic, Influence of rotor geometry on tip leakage and port flow areas in gerotor-type twin screw compressors, Proc. Inst. Mech. Eng. Part E: J. Process. Mech. Eng. 236 (1) (2020) 94–102, http://dx.doi.org/10.1177/0954408920962412.
[17] H. Lacevic, A. Kovacevic, M. Read, An investigation of internally geared screw compressor performance using a chamber modelling approach, in: M. Read, S. Rane, I. Ivkovic-Kihic, A. Kovacevic (Eds.), 13th International Conference on Compressors and their Systems, ICCS 2023, in: Springer Proceedings in Energy, Springer, Cham, 2024, http://dx.doi.org/10.1007/978-3-031-42663-6_40.
[18] M. Rundo, Models for flow rate simulation in gear pumps: A review, Energies 10 (9) (2017) 1261.
[19] A. Kovacevic, N. Stosic, I.K. Smith, Springer, Berlin, 2007.
[20] K. Vimalakanthan, M. Read, A. Kovacevic, Numerical modelling and experimental validation of twin-screw expanders, Energies 13 (18) (2020) 4700, http://dx.doi.org/10.3390/en13184700.
[21] J. Colbourne, The geometry of trochoid envelopes and their application in rotary pumps, Mech. Mach. Theory 9 (3–4) (1974) 421–435, http://dx.doi.org/10.1016/0094-114x(74)90025-1.
[22] D. Vecchiato, A. Demenego, J. Argyris, F.L. Litvin, Geometry of a cycloidal pump, Comput. Methods Appl. Mech. Engrg. 190 (18–19) (2001) 2309–2330, http://dx.doi.org/10.1016/s0045-7825(00)00236-x.
[23] O. Alipiev, S. Antonov, T. Grozeva, Generalized model of undercutting of involute spur gears generated by rack-cutters, Mech. Mach. Theory 64 (2013) 39–52, http://dx.doi.org/10.1016/j.mechmachtheory.2013.01.002.
[24] F.L. Litvin, A. Fuentes, Gear Geometry and Applied Theory, second ed., Cambridge University Press, Cambridge, 2004.
[25] H.W. Guggenheimer, Differential Geometry, Dover Publications, New York, 1977.
[26] I.A. Sakun, Screw Compressors, Mashgiz, Moscow, 1960, In Russian.
[27] N. Stosic, K. Hanjalic, Development and optimization of screw machines with a simulation model—Part I: Profile generation, J. Fluids Eng. 119 (3) (1997) 659–663, http://dx.doi.org/10.1115/1.2819295.
[28] J. Beard, D. Yannitell, G. Pennock, The effects of the generating pin size and placement on the curvature and displacement of epitrochoidal gerotors, Mech. Mach. Theory 27 (4) (1992) 373–389, http://dx.doi.org/10.1016/0094-114x(92)90030-l.
[29] S.-H. Tong, J. Yan, D.C.H. Yang, Design of deviation-function based gerotors, Mech. Mach. Theory 44 (8) (2009) 1595–1606, http://dx.doi.org/10.1016/j.mechmachtheory.2009.01.001.
[30] J. Yan, D.C.H. Yang, S.-H. Tong, On the generation of analytical noncircular multilobe internal pitch curves, J. Mech. Des. 130 (9) (2008) 092601, http://dx.doi.org/10.1115/1.2943298.
[31] D.C.H. Yang, J. Yan, S.-H. Tong, Flowrate formulation of deviation function based gerotor pumps, J. Mech. Des. 132 (6) (2010) 064503, http://dx.doi.org/10.1115/1.4001595.
[32] H. Cai, Z. Li, Y. Zhang, Design of gerotor oil pump with new rotor profile for improving performance, Proc. Inst. Mech. Eng. Part C: J. Mech. Eng. Sci. 229 (6) (2015) 1061–1071, http://dx.doi.org/10.1177/0954406215618228.
[33] M.R. Karamooz, Elliptical lobe shape gerotor pump design to minimize wear, Front. Mech. Eng. 6 (2011) 429–434, http://dx.doi.org/10.1007/s11465-011-0247-6.
[34] M.G. Read, N. Stosic, I.K. Smith, The influence of rotor geometry on power transfer between rotors in gerotor-type screw compressors, ASME J. Mech. Des. 142 (7) (2020) 073501, http://dx.doi.org/10.1115/1.4045508.
[35] H. Lacevic, A. Kovacevic, M. Read, Optimization of internally geared screw machine geometry for air compression application, in: Proceedings of the 25th International Compressor Engineering Conference At Purdue, West Lafayette, Indiana, 2024.
[36] A. Robison, Design of Gerotor Gear Geometry by Multi-Objective Optimization (Ph.D. thesis), (30504971) Purdue University, 2021.
[37] M. Read, Epitrochoidal gerotor profiles with asymmetric lobes, in: Proceedings of the 26th International Compressor Engineering Conference, West Lafayette, Indiana, 2022.
[38] D. Genta, G. Ghigo, M. Milanese, A. Pennacchi, Influence of rotor profile geometry on the performance of an original low-pressure gerotor pump, Mech. Mach. Theory 105 (2016) 245–261, http://dx.doi.org/10.1016/j.mechmachtheory.2016.02.012.
[39] H. Lacevic, A. Kovacevic, N. Stosic, M. Read, On rotor profiling of internally geared screw machines, IOP Conf. Ser.: Mater. Sci. Eng. 1322 (2024) 012006, http://dx.doi.org/10.1088/1757-899X/1322/1/012006.
[40] E. Buckingham, Analytical Mechanics of Gears, Dover Publications, New York, 1988, Reprint of the 1949 edition, McGraw-Hill Book Company, Inc..